Inorg. Chem. **2005**, *44*, 3356–3366

Gas-Phase Reactivity of Heterobinuclear Oxometalate Anions $[CrMoO_6(OR)]^-$, $[CrWO_6(OR)]^-$, and $[MoWO_6(OR)]^-$ (R = H, ^{n}Bu)

Tom Waters,* Richard A. J. O'Hair,* and Anthony G. Wedd

School of Chemistry, The University of Melbourne, Victoria, Australia, 3010

Received February 23, 2005

Heterobinuclear oxometalate anions based upon $[CrMoO_7]^{2-}$, $[CrWO_7]^{2-}$, and $[MoWO_7]^{2-}$ were generated and transferred to the gas phase by the electrospray process from acetonitrile solutions containing two of the salts $(Bu_4N)_2[MO_4]$ (M = Cr, Mo, W). Their reactivities were examined and compared with those of the related homobinuclear anions based upon $[M_2O_7]^{2-}$ (M = Cr, Mo, W). Particular emphasis was placed upon reactions relevant to gas-phase catalytic cycles described previously for oxidation of alcohols by $[Mo_2O_6(OH)]^-$ (Waters, T.; O'Hair, R. A. J.; Wedd, A. G. *J. Am. Chem. Soc.* **2003**, *125*, 3384–3396). The protonated anions $[MM'O_6(OH)]^-$ each reacted with methanol with loss of water to form $[MM'O_6(OCH_3)]^-$ at a rate that was intermediate between those of $[M_2O_6(OH)]^-$ and $[M'_2O_6(OH)]^-$. The butylated anions $[MM'O_6(OBu)]^-$ were generated by collisional activation of the ion-pairs $\{Bu_4N^+[MM'O_7]^{2-}\}^-$. Collisional activation of $[MM'O_6(OBu)]^-$ resulted in either the loss of butanal (redox reaction) or the loss of butene (elimination reaction), with the detailed nature of the observations depending on the nature of both M and M′. Selective ^{18}O labeling indicated that the butoxo ligands of $[CrMoO_6(OBu)]^-$ and $[CrWO_6(OBu)]^-$ were located on molybdenum and tungsten, respectively. This structural insight allowed a more detailed comparison of reactivity with the homobinuclear species, and highlighted the importance of the neighboring metal center in these reactions.

Introduction

Two gas-phase catalytic cycles for the oxidation of primary and secondary alcohols to aldehydes and ketones, respectively, were described recently.[1] The protonated dimolybdate anion $[Mo_2O_6(OH)]^-$ acted as catalyst in each cycle with nitromethane as oxidant (eq 1, Figure 1). The first cycle proceeds by three steps: (1) reaction of $[Mo_2O_6(OH)]^-$ with alcohol RR′HCOH and elimination of water to form $[Mo_2O_6(OCHRR')]^-$; (2) oxidation and elimination of the alkoxo ligand as the aldehyde or ketone RR′CO; and (3) regeneration of the catalyst by oxidation with nitromethane. Step (2) does not occur at room temperature and requires the use of collisional activation to proceed. The second cycle is similar but differs in the order of reaction with alcohol and nitromethane.

$$RR'CHOH + CH_3NO_2 \rightarrow RR'CO + H_2O + CH_3NO \quad (1)$$

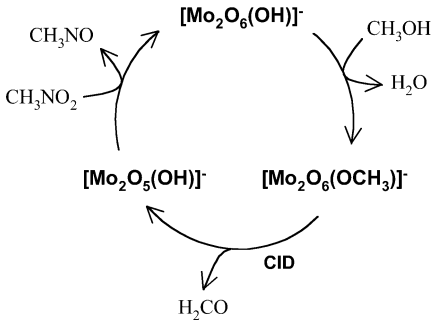

Figure 1. Gas-phase catalytic cycle for the oxidation of methanol to formaldehyde (eq 1).

The related mononuclear and binuclear anions $[MO_3(OH)]^-$ and $[M_2O_6(OH)]^-$ (M = Cr, Mo, W) were examined in parallel and significant differences in reactivity (acid−base, redox) were apparent as a function of both nuclearity and metal.[1,2] Only the dimolybdate center had the correct mix of properties needed to participate in each of the three steps of these catalytic cycles. These differences in reactivity

* Authors to whom correspondence should be addressed. E-mail: t.waters1@pgrad.unimelb.edu.au; rohair@unimelb.edu.au.

(1) Waters, T.; O'Hair, R. A. J.; Wedd, A. G. *J. Am. Chem. Soc.* **2003**, *125*, 3384−3396.

(2) Feyel, S.; Waters, T.; O'Hair, R. A. J.; Wedd, A. G. *J. Chem. Soc., Dalton Trans.* **2004**, 4010−4016.

10.1021/ic050288z CCC: $30.25
Published on Web 04/08/2005

suggested an investigation of the heteronuclear species $[MM'O_7]^{2-}$ (M = Cr, Mo, W; M ≠ M′).

Mixed metal oxide surfaces are involved in a wide variety of processes involving both acid−base and redox catalysis.[3,4] Generation of fundamental reactivity trends from gas-phase data on mixed metal oxide ions might provide insights into this important class of catalysts. While the reactivity of a variety of mixed metal cluster cations has been the focus of a number of studies,[5−16] there have been relatively few studies on mixed metal oxide ions.[17−21] Small bi- and trinuclear oxometalate cluster cations such as $MFeO_n^+$ (M = Co, V, n = 1−3) and $MFe_2O_4^+$ (M = Ti, V) were generated by reaction of the bare metal clusters MFe^+ and MFe_2^+ with oxygen atom transfer reagents such as ethylene oxide or dioxygen, but only limited reactivity studies were undertaken.[17−19] Larger heteronuclear oxometalate clusters $Al_xIn_yO_z^+$ were generated by laser vaporization of aluminum−indium oxides.[20] Their reactivity toward NO_2 and N_2O was intermediate between those of their homonuclear counterparts $Al_{x+y}O_z^+$ and $In_{x+y}O_z^+$. More recently, pure bismuth oxide cluster cations (e.g., $Bi_6O_9^+$) and molybdenum-doped derivatives (e.g., $Bi_6O_9MoO_3^+$) were shown to exhibit similar reactivities toward ethane, suggesting that the effect of the additional MoO_3 unit on reactivity was negligible.[21] Heats of formation have been estimated for the cations $CrMO_3^+$, $CrMO_4^+$, and $CrMO_5^+$ (M = Mo, W) generated from vapors of Cr_2O_3 in molybdenum and tungsten effusion cells, however no reactivity studies were reported.[22] Finally, heterometallic Nb/Ta alkoxides such as $NbTa(OEt)_9^+$ were generated by elecrospray of solutions containing both of $Nb(OEt)_5$ and $Ta(OEt)_5$.[23] Their structure and reactivity was examined by collisional activation experiments.

The present work reports the generation of heteronuclear oxometalate anions based upon $[MM'O_7]^{2-}$ (M, M′ = Cr, Mo, W; M ≠ M′). Their reactivity is compared with that of their homonuclear counterparts $[M_2O_7]^{2-}$. Isotope labeling studies identified the site of reaction in the heteronuclear anions.

Experimental Section

Synthesis. Tetra-*n*-butylammonium salts of mononuclear $[CrO_4]^{2-}$, $[MoO_4]^{2-}$, and $[WO_4]^{2-}$ and binuclear $[Cr_2O_7]^{2-}$ and $[Mo_2O_7]^{2-}$ were synthesized using standard literature methods.[24−28]

^{18}O labeled $(Bu_4N)_2[MO_4]$ were generated by dissolving $(Bu_4N)_2[MO_4]$ in a solution of $^{18}OH_2$ (95 atom % ^{18}O, Novachem) in dried acetonitrile (20% v/v) and incubating for approximately one week to ensure attainment of equilibrium. The level of ^{18}O label incorporation estimated for each of $[MO_4]^{2-}$ was 90−95% (see below), consistent with the content of the water employed.

Mass Spectrometry (MS). Experiments were carried out using a modified Finnigan LCQ quadrupole ion trap mass spectrometer equipped with a Finnigan electrospray ionization source. Solutions for electrospray were made to approximately 0.1 mg mL^{-1} in acetonitrile. Sample solutions were pumped into the electrospray source through fused silica tubing (i.d. 50 μm) at a flow rate of 3 μL/min. Typical conditions involved nitrogen sheath gas (30−70 psi), no auxiliary gas, and a spray voltage of 3−5 kV. The capillary voltage and the tube lens offset were tuned to maximize the signal of the desired ion. The capillary temperature was set at 200 °C.

Experiments involving collisional induced dissociation (CID) were performed by mass selecting target ions using standard isolation and excitation techniques. All data were collected over an average of at least 15 scans. Detailed descriptions of the instrumental modifications and experimental procedure used to measure ion−molecule reaction rate constants can be found elsewhere.[1]

Chromate, molybdate, and tungstate anions display distinctive isotope patterns due to the relative abundances of naturally occurring isotopes. This facilitates assignment of ion stoichiometry via comparison of experimental and theoretical isotopomer patterns (e.g., Figure 2). However, the broad isotope pattern can also make small mass changes difficult to detect (e.g., during isotope labeling experiments). To avoid this problem, a *single* peak in the isotopomer pattern was mass selected and used to follow the course of reactions.

Generation of Heterobinuclear Anions. Heterobinuclear anions based upon $[MM'O_7]^{2-}$ (M = Cr, Mo, W; M ≠ M′) were generated by the electrospray process from acetonitrile solutions containing approximately 0.1 mg mL^{-1} of two of the salts $(Bu_4N)_2[MO_4]$. These are presumably formed by a condensation reaction (eq 2). Sufficient signal intensity of each of the dianions $[MM'O_7]^{2-}$, the protonated anions $[MM'O_6(OH)]^-$, and the ion pairs $\{Bu_4N^+[MM'O_7]^{2-}\}^-$ could be generated to allow further experiments.

(3) Ertl, G., Knözinger, H., Weitkamp, J., Eds. *Handbook of Heterogeneous Catalysis*; Wiley: Weinheim, Germany, 1997; 2541 pp.
(4) Rao, C. N. R.; Raveau, B. *Transition Metal Oxides: Structure, Properties and Synthesis of Ceramic Oxides*, 2nd ed.; Wiley-VCH: Weinheim, Germany, 1998; 373 pp.
(5) Tews, E. C.; Freiser, B. S. *J. Am. Chem. Soc.* **1987**, *109*, 4433−4440.
(6) Huang, Y.; Freiser, B. S. *J. Am. Chem. Soc.* **1988**, *110*, 387−392.
(7) Lech, L. M.; Freiser, B. S.; Gord, J. R. *J. Am. Chem. Soc.* **1989**, *111*, 8588−8592.
(8) Roth, L. M.; Freiser, B. S.; Bauschlicher, C. W., Jr.; Partridge, H.; Langhoff, S. R. *J. Am. Chem. Soc.* **1991**, *113*, 3274−3280.
(9) Butcher, C. P. G.; Dinca, A.; Dyson, P. J.; Johnson, B. F. G.; Langridge-Smith, P. R. R.; McIndoe, J. S. *Angew. Chem., Int. Ed.* **2003**, *42*, 5752−5755.
(10) Nonose, S.; Sone, Y.; Onodera, K.; Sudo, S.; Kaya, K. *Chem. Phys. Lett.* **1989**, *164*, 427−432.
(11) Nonose, S.; Sone, Y.; Onodera, K.; Sudo, S.; Kaya, K. *J. Phys. Chem.* **1990**, *94*, 2744−2746.
(12) Harms, A. C.; Leuchtner, R. E.; Sigsworth, S. W.; Castleman, A. W., Jr. *J. Am. Chem. Soc.* **1990**, *112*, 5673−5674.
(13) Koszinowski, K.; Schröder, D.; Schwarz, H. *J. Am. Chem. Soc.* **2003**, *125*, 3676−3677.
(14) Koszinowski, K.; Schröder, D.; Schwarz, H. *ChemPhysChem* **2003**, *4*, 1233−1237.
(15) Koszinowski, K.; Schröder, D.; Schwarz, H. *Organometallics* **2004**, *23*, 1132−1139.
(16) Koszinowski, K.; Schröder, D.; Schwarz, H. *Angew. Chem., Int. Ed.* **2004**, *43*, 121−124.
(17) Hettich, R. L.; Freiser, B. S. *J. Am. Chem. Soc.* **1985**, *107*, 6222−6226.
(18) Jacobson, D. B.; Freiser, B. S. *J. Am. Chem. Soc.* **1986**, *108*, 27−30.
(19) Harvey, J. N.; Schroder, D.; Schwarz, H. *Inorg. Chim. Acta* **1998**, *273*, 111−115.
(20) Parent, D. C. *Chem. Phys. Lett.* **1991**, *183*, 51−54.
(21) Fielicke, A.; Rademann, K. *Chem. Phys. Lett.* **2002**, *359*, 360−366.
(22) Lopatin, S. I.; Shugurov, S. M.; Semenov, G. A. *Rapid Commun. Mass Spectrom.* **2004**, *18*, 112−116.
(23) Zemski, K. A.; Castleman, A. W., Jr.; Thorn, D. L. *J. Phys. Chem. B* **2001**, *105*, 4633−4639
(24) Nakayama, H. *Bull. Chem. Soc. Jpn.* **1983**, *56*, 877−880.
(25) Klemperer, W. G.; Liu, R. S. *Inorg. Chem.* **1980**, *19*, 3863−3864.
(26) Che, T. M.; Day, V. W.; Francesconi, L. C.; Fredrich, M. F.; Klemperer, W. G.; Shum, W. *Inorg. Chem.* **1985**, *24*, 4055−4062.
(27) Landini, D.; Rolla, F. *Chem. Ind.* **1979**, 213.
(28) Hur, N. H.; Klemperer, W. G.; Wang, R.-C. In *Inorganic Synthesis*; Ginsberg, A. P., Ed.; John Wiley & Sons: New York, 1990; Vol. 27, pp 79−80.

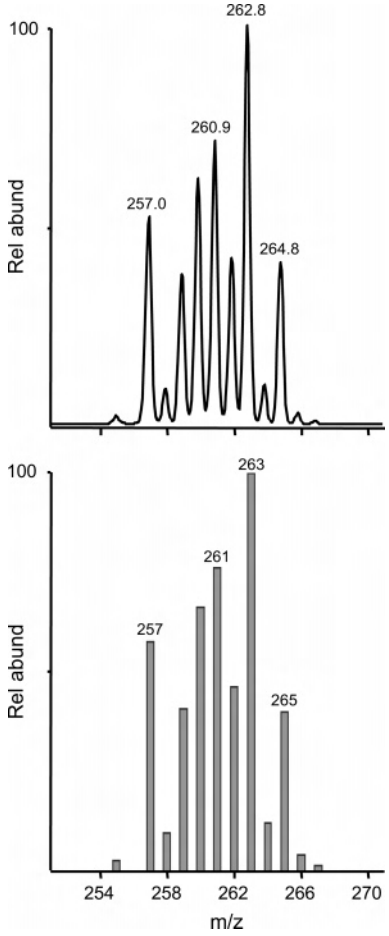

Figure 2. Comparison of experimental (above) and theoretical (below) isotope patterns for $[CrMoO_6(OH)]^-$. Selected peaks are labeled to aid comparison.

$$[MO_3(OH)]^- + [M'O_3(OH)]^- \rightarrow [MM'O_7]^{2-} + H_2O \quad (2)$$

Generation of ^{18}O-Labeled Heterobinuclear Anions. Heterobinuclear anions with the terminal oxo ligands of one metal center only labeled with ^{18}O were generated from solutions containing labeled $(Bu_4N)_2[M^{18}O_4]$ and unlabeled $(Bu_4N)_2[M'O_4]$ (e.g., $[CrMoO_7]^{2-}$, eq 3).

$$[Cr^{16}O_3(^{16}OH)]^- + [Mo^{18}O_3(^{18}OH)]^- \rightarrow [^{16}O_3Cr(^{16/18}O)Mo^{18}O_3]^{2-} + {}^{1618}OH_2 \quad (3)$$

Solutions of ^{18}O-labeled $(Bu_4N)_2[M^{18}O_4]$ in $^{18}OH_2$/MeCN (20% v/v) were diluted with dried MeCN to the optimal concentration for the electrospray process (~0.1 mg/mL). This approach meant that ^{18}O-labeled $(Bu_4N)_2[M^{18}O_4]$ did not have to be isolated in substance, but also meant that small amounts of free $^{18}OH_2$ was present in the electrospray solution (~1.25% v/v $^{18}OH_2$/MeCN). This introduced the possibility of label scrambling with unlabeled $(Bu_4N)_2[M'O_4]$. To suppress this, contact time between the labeled and unlabeled solutions was minimized by injecting the two solutions from separate syringes into a mixing tee-piece, and the mixed solution was injected directly into the electrospray source. Contact time between the two solutions was estimated as 5−10 s on the basis of solution flow-rates and the length and cross-section of the fused silica tubing used to connect the mixing apparatus and the electrospray source. In addition, the approach also ensured that contact time between the two solutions was maintained at a constant value throughout the experiments. Trial experiments with unlabeled anions indicated that heteronuclear anions could be generated by this method, but with lower current intensities and poorer signal stability than from the conventional single syringe. Experimental details for the composition of labeled and unlabeled solutions used in the experiments are outlined in Table 1.

The extent of ^{18}O label incorporation was estimated by fitting theoretical isotope patterns generated by varying ^{18}O label incorporation to the experimental isotope pattern. The isotope patterns for the mononuclear species $[MO_3(OH)]^-$ often contained interference from overlap with $[MO_4]^-$, complicating an accurate estimate of ^{18}O label incorporation for this ion. Instead, the binuclear anion $[M_2O_6(OBu)]^-$ was chosen as a representative species to estimate ^{18}O incorporation as it could be generated from the ion pair $\{Bu_4N^+[M_2O_7]^{2-}\}^-$ in high yield and free from overlapping peaks (see below, eq 5). The ^{18}O label content of this ion is expected to accurately reflect the label content of $[MO_4]^{2-}$ in solution. Estimated ^{18}O label incorporation for mononuclear $[MO_4]^{2-}$ in each of the experiments is detailed in Table 1. Comparisons between experimental and theoretical isotope patterns for selectively labeled species can be found in the Supporting Information.

Theoretical Calculations. Hybrid density functional theory (DFT) calculations employing the B3LYP functional were carried out using the Gaussian 03 program.[29] The 6-311++G** basis sets were used for hydrogen, carbon, and oxygen, whereas the effective core potential of Stevens et al was used for chromium, molybdenum, and tungsten.[30] Unscaled zero point energies are included for all species. Structures were visualized using MacMolPlt.[31] Cartesian coordinates and energies of optimized geometries for isomers of $[MM'O_6(OCH_3)]^-$ (M, M′ = Cr, Mo, W; M ≠ M′) are included in the Supporting Information (Figures S1−S3).

Results

Generation of Heteronuclear Anions. Although both dichromate and dimolybdate are readily available, the ditungstate dianion has not been isolated in the condensed phase. However, it can be generated by the electrospray process from acetonitrile solutions of $(Bu_4N)_2[WO_4]$, and is presumably formed via condensation of two tungstate centers (c.f, eq 2).[1,32,33] Heterobinuclear anions based upon $[MM'O_7]^{2-}$ were generated by a similar approach involving acetonitrile

(29) Frisch, M. J.; Trucks, G. W.; Schlegel, H. B.; Scuseria, G. E.; Robb, M. A.; Cheeseman, J. R.; Montgomery, J. A., Jr.; Vreven, T.; Kudin, K. N.; Burant, J. C.; Millam, J. M.; Iyengar, S. S.; Tomasi, J.; Barone, V.; Mennucci, B.; Cossi, M.; Scalmani, G.; Rega, N.; Petersson, G. A.; Nakatsuji, H.; Hada, M.; Ehara, M.; Toyota, K.; Fukuda, R.; Hasegawa, J.; Ishida, M.; Nakajima, T.; Honda, Y.; Kitao, O.; Nakai, H.; Klene, M.; Li, X.; Knox, J. E.; Hratchian, H. P.; Cross, J. B.; Adamo, C.; Jaramillo, J.; Gomperts, R.; Stratmann, R. E.; Yazyev, O.; Austin, A. J.; Cammi, R.; Pomelli, C.; Ochterski, J. W.; Ayala, P. Y.; Morokuma, K.; Voth, G. A.; Salvador, P.; Dannenberg, J. J.; Zakrzewski, V. G.; Dapprich, S.; Daniels, A. D.; Strain, M. C.; Farkas, O.; Malick, D. K.; Rabuck, A. D.; Raghavachari, K.; Foresman, J. B.; Ortiz, J. V.; Cui, Q.; Baboul, A. G.; Clifford, S.; Cioslowski, J.; Stefanov, B. B.; Liu, G.; Liashenko, A.; Piskorz, P.; Komaromi, I.; Martin, R. L.; Fox, D. J.; Keith, T.; Al-Laham, M. A.; Peng, C. Y.; Nanayakkara, A.; Challacombe, M.; Gill, P. M. W.; Johnson, B.; Chen, W.; Wong, M. W.; Gonzalez, C.; Pople, J. A. *Gaussian 03*, revision B.04; Gaussian, Inc.: Wallingford, CT, 2004.
(30) Stevens, W. J.; Krauss, M.; Basch, H.; Jasien, P. G. *Can. J. Chem.* **1992**, *70*, 612−630.
(31) Bode, B. M.; Gordon, M. S. *J. Mol. Graphics Modell.* **1998**, *16*, 133−138.
(32) Deery, M. J.; Howarth, O. W.; Jennings, K. R. *J. Chem. Soc., Dalton Trans.* **1997**, 4783−4788.
(33) Truebenbach, C. S.; Houalla, M.; Hercules, D. M. *J. Mass Spectrom.* **2000**, *35*, 1121−1127.

Table 1. Composition of MeCN Solutions and ^{18}O Label Content of Anions Used to Generate Selectively Labelled $[CrMO_6(OBu)]^-$ (M = Mo, W)[a,b]

	Composition of Electrospray Solutions		^{18}O Content (atom %)	
experiment	syringe 1	syringe 2	$[CrO_4]^{2-}$	$[MO_4]^{2-}$
1	$(Bu_4N)_2[CrO_4]$	$(Bu_4N)_2[Mo^{18}O_4]$ + 1.25% $^{18}OH_2$	0	92
2	$(Bu_4N)_2[Cr^{18}O_4]$ + 1.25% $^{18}OH_2$	$(Bu_4N)_2[MoO_4]$	93	87
3	$(Bu_4N)_2[Cr^{18}O_4]$ + 1.25% $^{18}OH_2$	$(Bu_4N)_2[MoO_4]$ + 12.5% $^{16}OH_2$	92	8
4	$(Bu_4N)_2[CrO_4]$	$(Bu_4N)_2[W^{18}O_4]$ + 1.25% $^{18}OH_2$	0	93
5	$(Bu_4N)_2[Cr^{18}O_4]$ + 1.25% $^{18}OH_2$	$(Bu_4N)_2[WO_4]$	93	89
6	$(Bu_4N)_2[Cr^{18}O_4]$ + 1.25% $^{18}OH_2$	$(Bu_4N)_2[WO_4]$ + 3.75% $^{16}OH_2$	93	20

[a] The assigned label content of $[CrO_4]^{2-}$ and $[MO_4]^{2-}$ was estimated from $[Cr_2O_6(OBu)]^-$ and $[M_2O_6(OBu)]^-$, respectively. The assigned label content of $[CrMO_6(OBu)]^-$ is detailed in Table 5. [b] The concentration of $(Bu_4N)_2[CrO_4]$ and $(Bu_4N)_2[MO_4]$ in each syringe was 0.1 mg/mL. The content of $^{16}OH_2$ and $^{18}OH_2$ in each syringe is expressed as %v/v H_2O/MeCN.

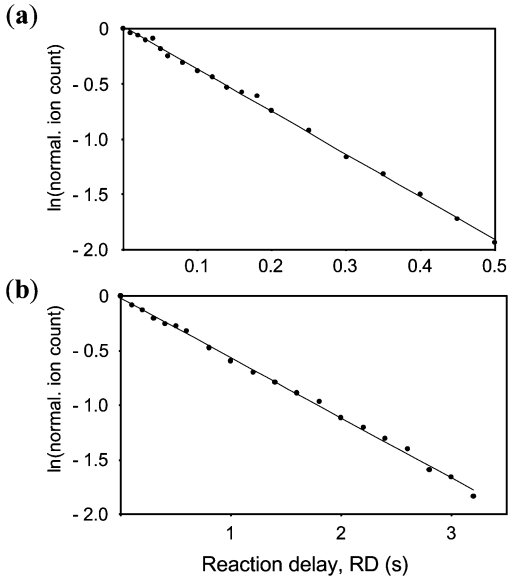

Figure 3. First order plots for reaction of (a) $[CrWO_6(OH)]^-$ with CH_3OH, and (b) $[CrWO_6(OBu)]^-$ with CH_3OH. The partial pressures of CH_3OH were 2.5×10^{12} and 3.8×10^{11} molecules cm^{-3}, respectively.

solutions containing a mixture of $(Bu_4N)_2[MO_4]$ and $(Bu_4N)_2[M'O_4]$ (eq 2). For example, an equimolar mixture of $(Bu_4N)_2[CrO_4]$ and $(Bu_4N)_2[MoO_4]$ yielded peaks assigned to the dianion $[CrMoO_7]^{2-}$, its protonated form $[CrMoO_6(OH)]^-$, and the ion pair $\{Bu_4N^+[CrMoO_7]^{2-}\}^-$. Equivalent species based upon $[CrWO_7]^{2-}$ and $[MoWO_7]^{2-}$ could be generated, and sufficient yields of each allowed further investigation of their reactivity.

The composition of heterobinuclear anions was determined by comparison of experimental and theoretical isotope patterns. The significantly different masses and relative abundances of the naturally occurring isotopes of chromium, molybdenum, and tungsten allowed an unequivocal assignment of the metal composition of these species (e.g., Figure 2, $[CrMoO_6(OH)]^-$).

Reaction of $[MM'O_6(OH)]^-$ with Methanol. Each of the anions $[MM'O_6(OH)]^-$ reacted with methanol to form $[MM'O_6(OCH_3)]^-$ with loss of water (eq 4) in a reaction equivalent to that observed for $[Mo_2O_6(OH)]^-$.[1]

$$[MM'O_6(OH)]^- + CH_3OH \rightarrow [MM'O_6(OCH_3)]^- + H_2O \quad (4)$$

These reactions all followed smooth pseudo-first-order kinetics (e.g., Figure 3a for $[CrWO_6(OH)]^-$). Rate constants for the heterobinuclear anions $[MM'O_6(OH)]^-$ and the equivalent homobinuclear anions $[M_2O_6(OH)]^-$ are listed in Table 2.[1,34] The reactivities of the heterobinuclear centers were intermediate between those of their respective homobinuclear counterparts (Table 2).

Table 2. Reaction Rates for the Reaction of $[MM'O_6(OR)]^-$ with MeOH[a]

R	MM′	rate[b]	ϕ[c]
H	Cr_2	<0.001	<0.00001
	CrMo	~0.004	~0.00003
	CrW	0.14	0.0010
	Mo_2	6.9	0.049
	MoW	20	0.14
	W_2	78	0.57
Bu	Cr_2	<0.001	<0.00001
	CrMo	~0.004	~0.00003
	CrW	0.15	0.0011
	Mo_2	2.3	0.017
	MoW	6.2	0.045
	W_2	13	0.095

[a] Data for $[M_2O_6(OH)]^-$ are taken from ref 1. [b] $\times 10^{-11}$ cm^3 $molecule^{-1}$ s^{-1}. [c] Reaction efficiency, $\phi = k_{exp}/k_{ADO}$.

The presence of chromium in $[CrMoO_6(OH)]^-$ and $[CrWO_6(OH)]^-$ induced a dramatic decrease in reactivity relative to that of $[Mo_2O_6(OH)]^-$ and $[W_2O_6(OH)]^-$, respectively. $[CrMoO_6(OH)]^-$ reacted extremely slowly with methanol. The experimental rate constant of $\sim 4 \times 10^{-14}$ cm^3 $molecule^{-1}$ s^{-1} was slightly higher than the upper limit estimated for protonated dichromate $[Cr_2O_6(OH)]^-$,[34] but is 3 orders of magnitude lower than that for $[Mo_2O_6(OH)]^-$. Qualitatively similar observations are apparent for $[CrWO_6(OH)]^-$, which was significantly more reactive than $[Cr_2O_6(OH)]^-$, but about 500-fold less reactive than $[W_2O_6(OH)]^-$. The reaction rate observed for $[MoWO_6(OH)]^-$ was also intermediate between those of $[Mo_2O_6(OH)]^-$ and $[W_2O_6(OH)]^-$ (Table 2).

These kinetic data revealed that each metal center in $[MM'O_6(OH)]^-$ has a significant effect on reactivity toward methanol. In particular, the presence of the more electronegative chromium atom appears to reduce significantly the basicity of ligand hydroxo and its ability to abstract the proton from methanol required for elimination of water.

Reaction of $[MM'O_6(OBu)]^-$ with Methanol. The butoxo anions $[MM'O_6(OBu)]^-$ were generated by collisional activa-

(34) The upper bound for the rate constant of reaction between $[Cr_2O_6(OH)]^-$ and CH_3OH was estimated previously as $<5 \times 10^{-14}$ cm^3 $molecule^{-1}$ s^{-1}. This has been lowered further to $<1 \times 10^{-14}$ cm^3 $molecule^{-1}$ s^{-1} by using higher concentrations of methanol. This allows the slow reaction observed for $[CrMoO_6(OH)]^-$ ($k \approx 4 \times 10^{-14}$ cm^3 $molecule^{-1}$ s^{-1}) to be distinguished from the lack of reaction observed for $[Cr_2O_6(OH)]^-$.

Table 3. Branching Ratio for Collisional Activation of $[MM'O_6(OBu)]^-$ Anions[a]

MM′	loss of butanal	loss of butene
Cr_2	100	0
CrMo	100	0
CrW	100	0
Mo_2	97	3
MoW	80	20
W_2	0	100

[a] Data for $[M_2O_6(OBu)]^-$ are taken from ref 1.

tion of the respective ion-pairs $\{Bu_4N^+[MM'O_7]^{2-}\}^-$ (eq 5), a reaction equivalent to that described previously for the dimolybdate ion pair $\{Bu_4N^+[M_2O_7]^{2-}\}^-$.[1] Each of the butoxo anions reacted with methanol to form $[MM'O_6(OCH_3)]^-$ with loss of butanol (eq 6). These reactions all followed smooth pseudo-first-order kinetics (e.g., Figure 3b for $[CrWO_6(OBu)]^-$), and rate constants are given in Table 2. An additional clustering reaction was observed for the ditungstate anion, presumably the result of a stabilizing termolecular collision between the ion−molecule complex $\{[W_2O_6(OBu)]\cdots CH_3OH\}^-$ and a helium atom (eq 7).

$$\{Bu_4N^+[MM'O_7]^{2-}\}^- \rightarrow [MM'O_6(OBu)]^- + NBu_3 \quad (5)$$

$$[MM'O_6(OBu)]^- + CH_3OH \rightarrow [MM'O_6(OCH_3)]^- + BuOH \quad (6)$$

$$[W_2O_6(OBu)]^- + CH_3OH \rightarrow \{[W_2O_6(OBu)]\cdots CH_3OH\}^- \quad (7)$$

The qualitative observations for reaction of $[MM'O_6(OBu)]^-$ with methanol were analogous to those described above for $[MM'O_6(OH)]^-$; i.e., species containing a chromium center were relatively unreactive and rate constants for the heteronuclear species were intermediate between those of the relevant homonuclear species.

Collisional Activation of $[MM'O_6(OBu)]^-$. Mass selection and collisional activation of the butoxo anions $[MM'O_6(OBu)]^-$ revealed competition between oxidation and loss of the butoxo ligand as butanal (eq 8) and the non-redox elimination of butene (eq 9). Branching ratios for each of the homobinuclear and heterobinuclear centers are summarized in Table 3. No significant differences in branching ratio were detected as a function of collision energy. The product ion from loss of butanal corresponds to an ion of stoichiometry $[M, M', O_6, H]^-$. Two isomers were proposed for the dimolybdate analogue on the basis of theoretical calculations and the experimentally observed reactivity.[1] These were assigned to a reduced Mo^V_2 center with ligand hydroxo $[Mo^V_2O_5(OH)]^-$ and an oxidized Mo^{VI}_2 center with ligand hydrido $[HMo_2O_6]^-$. The presence of different metal centers in $[M, M', O_6, H]^-$ introduces an additional complication, and the structure of these product ions is not considered further.

$$[MM'O_6(OBu)]^- \rightarrow [M, M', O_6, H]^- + CH_3CH_2CH_2CH{=}O \quad (8)$$

$$\rightarrow [MM'O_6(OH)]^- + CH_3CH_2CH{=}CH_2 \quad (9)$$

$[CrMoO_6(OBu)]^-$ eliminated the butoxo ligand as butanal in a reaction that is equivalent to that observed previously for $[Cr_2O_6(OBu)]^-$ and $[Mo_2O_6(OBu)]^-$.[1] Similarly, $[CrWO_6(OBu)]^-$ eliminated butanal in a reaction equivalent to that observed for $[Cr_2O_6(OBu)]^-$ but in contrast with the loss of butene from $[W_2O_6(OBu)]^-$ (Table 3). These observations indicated that the presence of the stronger oxidant chromium in $[CrWO_6(OBu)]^-$ promoted aldehyde elimination and dominated the tendency of tungsten to eliminate alkene. $[MoWO_6(OBu)]^-$ eliminated both butanal and butene, with the former pathway dominating. This behavior was intermediate between that of $[Mo_2O_6(OBu)]^-$ (almost exclusive loss of butanal) and $[W_2O_6(OBu)]^-$ (exclusive loss of butene, Table 3).

Oxidation of $[M, M', O_6, H]^-$ with CH_3NO_2. The molybdenum analogue $[Mo_2, O_6, H]^-$ was assigned to a mixture of two isomers on the basis of experimentally observed reactivity and DFT calculations. Approximately 80% of the $[Mo_2, O_6, H]^-$ ion population reacted with nitromethane to yield $[Mo^{VI}_2O_6(OH)]^-$ and close the catalytic cycle for the oxidation of alcohols (eq 10; Figure 1).[1] This was assigned to the reduced hydroxo isomer $[Mo^V_2O_5(OH)]^-$. Approximately 20% of the $[Mo_2, O_6, H]^-$ ion population was unreactive toward nitromethane, and this was assigned to the oxidized hydrido isomer $[Mo^{VI}_2O_6H]^-$. DFT calculations predicted these two isomers to be very similar in energy. Calculations predicted the hydroxo isomer $[Cr^V_2O_5(OH)]^-$ was favored for chromium, and the lack of reaction of $[Cr^V_2O_5(OH)]^-$ with nitromethane was attributed to it being a poorer reductant than $[Mo^V_2O_5(OH)]^-$. In contrast, calculations predicted the hydrido isomer $[W^{VI}_2O_6H]^-$ was favored for tungsten, and its lack of reaction with nitromethane was attributed to its maximum oxidation state. The reactivity of the mixed metal equivalents $[M, M', O_6, H]^-$ toward CH_3NO_2 was examined to investigate their reactivity in the final step in the catalytic cycle (Figure 1) and to investigate the possibility of isomeric forms.

$$[Mo_2O_5(OH)]^- + CH_3NO_2 \rightarrow [Mo_2O_6(OH)]^- + CH_3NO \quad (10)$$

Neither $[Cr, Mo, O_6, H]^-$ nor $[Cr, W, O_6, H]^-$ reacted with CH_3NO_2, allowing an upper bound to be placed on their rate constants ($k < 5 \times 10^{-14}$ cm^3 molecule^{-1} s^{-1}). This was consistent with the lack of reaction observed for the chromium analogue $[Cr^V_2O_5(OH)]^-$.[1] In contrast, approximately 50% of the $[Mo, W, O_6, H]^-$ ion population reacted with nitromethane to yield $[MoWO_6(OH)]^-$, with the remaining 50% being unreactive. The observations of reactive and unreactive components were consistent with similar observations for $[Mo_2, O_6, H]^-$.[1] The reaction rate for the reactive component of $[Mo, W, O_6, H]^-$ appeared close to that of the collision rate ($k \approx 1.5 \times 10^{-9}$ cm^3 molecule^{-1} s^{-1}), although a more accurate measurement was not attempted.

Site of Reaction in Heteronuclear Species. The experiments detailed above described differences in reactivity between protonated and alkylated heteronuclear anions and their respective homonuclear counterparts. A more detailed

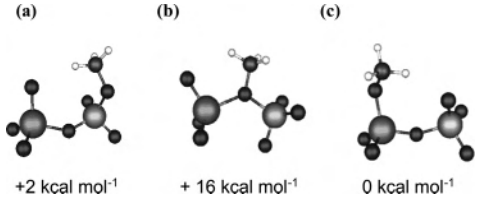

Figure 4. Predicted structural isomers and relative energies for $[CrMoO_6(OCH_3)]^-$: (a) the methoxo ligand at a chromium terminal site, (b) the methoxo ligand at the bridging site, and (c) the methoxo ligand at a molybdenum terminal site.

Table 4. DFT Predicted Relative Energies (kcal mol^{-1}) for Different Isomers of $[MM'O_6(OCH_3)]^-$

		Location of Methoxo Ligand		
M	M′	terminal M	bridging	terminal M′
Cr	Mo	2	16	0
Cr	W	4	20	0
Mo	W	2	25	0

interpretation of this reactivity is complicated by the possibility of different structural isomers of $[MM'O_6(OR)]^-$. For example, although collisional activation of the ion pairs $\{Bu_4N^+[MM'O_7]^{2-}\}^-$ (eq 5) resulted in S_N2 alkylation to yield $[MM'O_6(OBu)]^-$, the site of alkylation is unclear. This is illustrated for the case of $\{Bu_4N^+[CrMoO_7]^{2-}\}^-$ where alkylation might occur at a chromium oxo ligand, a molybdenum oxo ligand, or at the bridging oxo ligand. Each possibility would give rise to an isomer of $[CrMoO_6(OBu)]^-$ with the butoxo ligand at a different site. This situation contrasts with previous studies of dianion−tetraalkylammonium cation ion pairs in which the dianion was designed so that only one of the anionic centers was nucleophilic, thus ensuring reaction occurred at this site.[35,36]

Theoretical calculations based on density functional theory (DFT) were employed to provide insights into the relative stability of different structural isomers of $[MM'O_6(OR)]^-$. Calculations were carried out for the methoxo equivalent $[MM'O_6(OCH_3)]^-$ in order to reduce computational expense (Figure 4, Table 4, Figures S1−S3 in the Supporting Information). These indicated that the isomer with the methoxo ligand located at the bridging site was disfavored by at least 16 kcal mol^{-1} (Table 4). The most stable isomer (by 2−4 kcal mol^{-1}) in each system was predicted to be the one with a terminal methoxo ligand on the least electronegative metal center (Sanderson electronegativity:[38] W^{VI}, 1.67 < Mo^{VI}, 2.20 < Cr^{VI}, 3.37). However, the similar predicted energies for isomers with methoxo ligands at different terminal sites suggested an experimental probe was required to investigate this further.

Isotope labeling experiments based upon reaction with alcohol and elimination of aldehyde from $[MM'O_6(OBu)]^-$ (eqs 6 and 8) were employed to investigate the site of the butoxo ligand. These experiments involved selective ^{18}O labeling of the terminal oxo ligands of one metal center only. The method is based upon previous observations that collisional activation of $[Mo_2O_6(^{18}OCH_3)]^-$ resulted in loss of $^{18}OCH_2$ and reaction of $[Mo_2O_6(OBu)]^-$ with $CH_3{}^{18}OH$ resulted in formation of $[Mo_2O_6(^{18}OCH_3)]^-$ with loss of $Bu^{16}OH$.[1] The oxygen of the alkoxo ligand is lost in both cases. Scheme 1 outlines the approach for the specific case of loss of butanal from $[CrMoO_6(OBu)]^-$ labeled at the molybdenum oxo ligands.

Selectively labeled species were generated by the electrospray process from solutions containing ^{18}O labeled $(Bu_4N)_2[MO_4]$ and unlabeled $(Bu_4N)_2[M'O_4]$. This is illustrated for the example of $[CrMoO_7]^{2-}$ labeled at molybdenum. The methodology developed entailed injection of separate solutions of unlabeled $[CrO_4]^{2-}$ and ^{18}O-labeled $[MoO_4]^{2-}$ (∼92 atom %) at equal flow-rates into a mixing tee-piece, followed by direct transfer of the mixed solution into the electrospray source. Both of the homonuclear ion-pairs $\{Bu_4N^+[Cr_2O_7]^{2-}\}^-$ and $\{Bu_4N^+[Mo_2O_7]^{2-}\}^-$ as well as the heteronuclear ion pair $\{Bu_4N^+[CrMoO_7]^{2-}\}^-$ were generated by this method. The yield of the heteronuclear ion pair was significantly less than that obtained by direct injection of a mixture of the two solutions, however sufficient signal intensity could be obtained to allow for further experiments. The composition of the solutions used in each of the experiments is detailed in Table 1.

The ^{18}O label content of $[MO_4]^{2-}$ in solution was estimated from the respective butoxo species $[M_2O_6(OBu)]^-$. These ions were chosen as they could be generated cleanly from the ion-pairs $\{Bu_4N^+[M_2O_7]^-$ in high yield and free from overlapping peaks (eq 5). Fitting of the isotope patterns indicated that the ^{18}O contents of $[Cr_2O_6(OBu)]^-$ and $[Mo_2O_6(OBu)]^-$ were 0 and 92 atom %, respectively (Figure 5a and b). These values provided an indication of the ^{18}O label content of $[CrO_4]^{2-}$ and $[MoO_4]^{2-}$ in solution (Table 1, expt 1). The absence of ^{18}O label incorporation into $[Cr_2O_6(OBu)]^-$ indicated that $[CrO_4]^{2-}$ did not undergo exchange with free $^{18}OH_2$ present in the $[MoO_4]^{2-}$ solution on the time scale of the experiment (Table 1, expt 1).

The isotope pattern for $[CrMoO_6(OBu)]^-$ was fitted by assuming the label incorporation of the terminal oxo ligands of the chromium and molybdenum centers was equivalent to that estimated for mononuclear $[CrO_4]^{2-}$ and $[MoO_4]^{2-}$, respectively, in solution.[37] This assumption was consistent with the condensation mechanism proposed for formation of these species (eq 2). This indicated no label incorporation at the chromium terminal oxo ligand sites CrO_t and 92 % label incorporation at the molybdenum terminal oxo ligand sites MoO_t (Table 5, expt 1). The label incorporation of the single bridging oxo ligand was estimated by fitting of the theoretical isotope pattern generated using the above estimates for CrO_t and MoO_t and by varying CrO_bMo to fit the experimental isotope pattern. This suggested 15 % incorporation at the bridging oxo ligand site (Table 5). The theoretical isotope pattern generated on the basis of these estimates was in good agreement with the experimental isotope pattern

(35) Gronert, S.; Azebu, J. *Org. Lett.* **1999**, *1*, 503−506.
(36) Gronert, S.; Fong, L.-M. *Aust. J. Chem.* **2003**, *56*, 379−383.
(37) The label content of species based upon $[MM'O_7]^{2-}$ might also be examined by cluster fragmentation to generate two mononuclear species. However, such fragmentation is not observed under the present experimental conditions, with collisional activation resulting in either the loss of neutral fragments (e.g., eq 8) or no fragmentation. Attempts to use higher collisional activation energies to induce cluster fragmentation only resulted in loss of ion signal, most likely due to significant loss of ions from the ion trap.
(38) Huhey, J. E.; Keiter, E. A.; Keiter, R. L. *Inorganic Chemistry*, 4th ed.; Harper-Collins: New York, 1993; pp 188−190

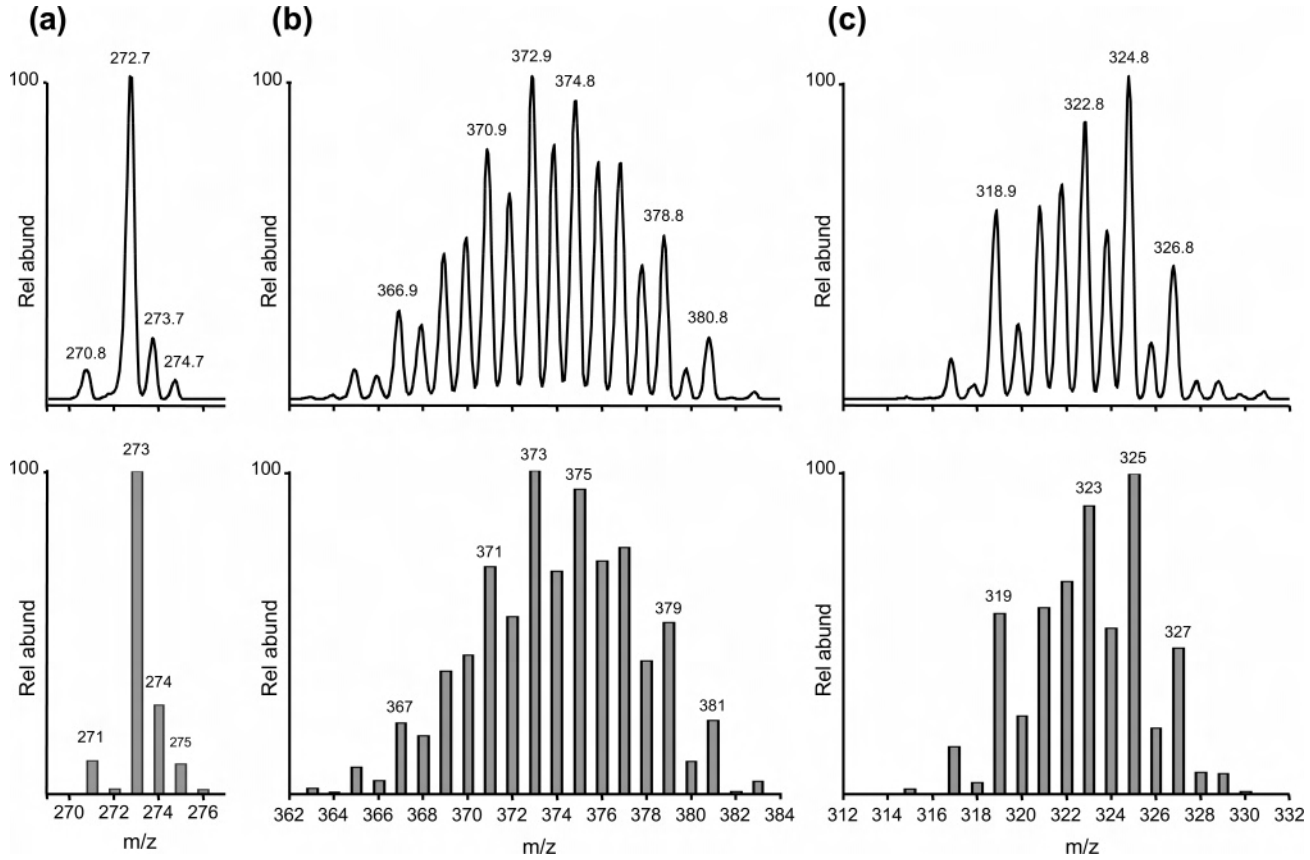

Figure 5. Experimental (above) and theoretical (below) isotope patterns for binuclear ions generated from a solution of $(Bu_4N)_2[CrO_4]$ (natural abundance) and $(Bu_4N)_2[MoO_4]$ (92 atom% ^{18}O) in MeCN (Table 1, expt 1). (a) $[Cr_2O_6(OBu)]^-$: theoretical isotope pattern generated assuming ^{18}O incorporation of 0 atom%. (b) $[Mo_2O_6(OBu)]^-$: theoretical isotope pattern generated assuming ^{18}O incorporation of 92 atom%. (c) $[CrMoO_6(OBu)]^-$: theoretical isotope pattern generated assuming ^{18}O incorporation of 0 atom% at CrO_t, 92 atom% at MoO_t and 15 atom% at CrO_bMo (Table 5, expt 1).

Scheme 1

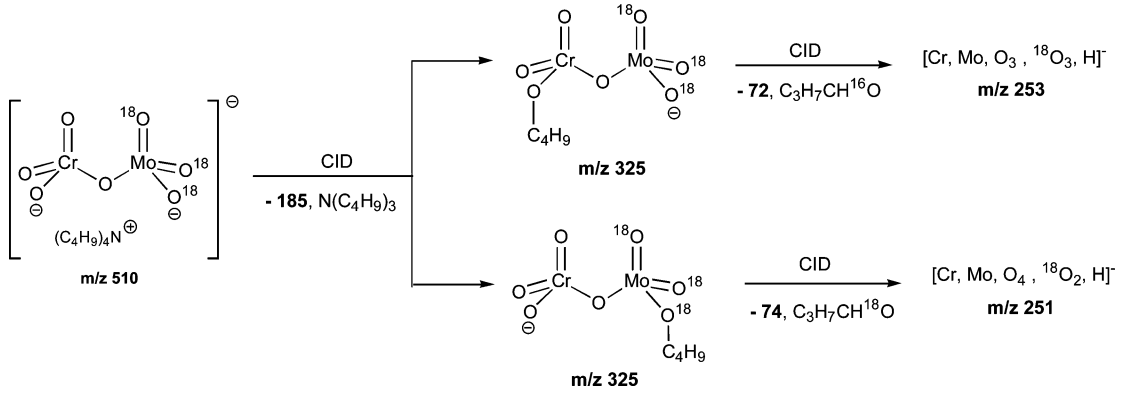

(Figure 5c). An equivalent theoretical isotope pattern could conceivably be generated by switching the estimates for CrO_t and MoO_t sites, however this would be inconsistent with the experimentally observed label content of $[CrO_4]^{2-}$ and $[MoO_4]^{2-}$ in solution.

Attempts to generate $[CrMoO_6(OBu)]^-$ labeled at the chromium terminal oxo ligand sites were complicated by exchange of unlabeled molybdate with free $^{18}OH_2$ in the labeled $[CrO_4]^{2-}$ solution following mixing. Initial experiments generated $[Mo_2O_6(OBu)]^-$ with an estimated label incorporation of 87%, indicating that unlabeled $[MoO_4]^{2-}$ in solution underwent almost complete exchange with free $^{18}OH_2$ in solution following mixing (Table 1, expt 2). This was consistent with the significantly faster rate of exchange expected for $[MoO_4]^{2-}$ compared with $[CrO_4]^{2-}$.[39,40]

Unwanted labeling of $[MoO_4]^{2-}$ was suppressed by inclusion of a 10-fold excess of $^{16}OH_2$ in the precursor $[MoO_4]^{2-}$ solution (Table 1, expt 3). This significantly reduced the extent of unwanted labeling of $[MoO_4]^{2-}$ in solution, with the label incorporation of $[Mo_2O_6(OBu)]^-$ estimated as 8%. Furthermore, the label incorporation of $[Cr_2O_6(OBu)]^-$ was

(39) Hinch, G. D.; Wycoff, D. E.; Murmann, R. K. *Polyhedron* **1986**, *5*, 487−495.
(40) Gamsjäger, H.; Murmann, R. K. Oxygen-18 Exchange Studies of Aqua and Oxo-ions. In *Advances in Inorganic and Bioinorganic Mechanisms*; Sykes, A. G., Ed.; Academic Press: London, 1983; Vol. 2, p 317−380.

Table 5. Estimated Level of ^{18}O Incorporation (atom %) into Anions $[CrMO_6(OBu)]^-$ (M = Mo, W)[a]

	^{18}O Incorporation		
experiment	CrO_t	CrO_bM	MO_t
1	0	15	92
2	93	90	87
3	92	90	8
4	0	20	93
5	93	90	89
6	93	85	20

[a] Experiments 1−3 M = Mo, experiments 4−6 M = W.

maintained at 92%, consistent with minimal exchange of labeled $[Cr^{18}O_4]^{2-}$ with the excess of free $^{16}OH_2$ present in solution following mixing. These data were consistent with the significantly slower rate of exchange expected for $[CrO_4]^{2-}$ compared with $[MoO_4]^{2-}$.[39,40] The experimental isotope pattern for $[CrMoO_6(OBu)]^-$ was fitted assuming ^{18}O incorporation of 92 % at CrO_t, 8 % at MoO_t, and 90 % at CrO_bMo (Table 5 expt 3, Figure S5).

Equivalent techniques were used to generate and assign the ^{18}O content for $[CrWO_6(OBu)]^-$ and results are summarized in Tables 1 and 5 and Figure S6. The signal for the ion-pair species $\{Bu_4N^+[CrWO_7]^{2-}\}^-$ was considerably weaker than that observed for $\{Bu_4N^+[CrMoO_7]^{2-}\}^-$, and was further reduced by the presence of the excess water in the electrospray solution. The conditions used represented a compromise between suppression of unwanted labeling and acceptable ion intensity. While the tungsten center could be labeled specifically (Tables 1 and 5; expt 4), labeling of the chromium center was accompanied by 20% labeling of the tungsten (Tables 1 and 5; expt 6). This was, however, adequate to distinguish between the two sites.

The experiments described above exploited the fact that $[CrO_4]^{2-}$ undergoes exchange with solvent water at a rate that is significantly slower than those of $[MoO_4]^{2-}$ and $[WO_4]^{2-}$.[39,40] Consequently, the rapid and similar rate of exchange of $[MoO_4]^{2-}$ and $[WO_4]^{2-}$ meant that the anion $[MoWO_6(OBu)]^-$ could not be labeled selectively by this procedure.

Collisional Activation of Labeled $[CrMO_6(OBu)]^-$. Access to $[CrMoO_6(OBu)]^-$ and $[CrWO_6(OBu)]^-$ labeled selectively at the terminal oxo ligands of one metal allowed the site of the butoxo ligand to be probed by elimination of butanal (e.g., Scheme 1).

Collisional activation of $[CrMoO_6(OBu)]^-$ generated from $\{Bu_4N^+[CrMoO_7]^{2-}\}^-$ labeled at molybdenum (MoO_t, 92 atom % ^{18}O) resulted in a mass loss of 74 Da (Figure 6a), consistent with elimination of ^{18}O-butanal (Scheme 1). The weaker peak corresponding to a mass loss of 72 Da is consistent with loss of ^{16}O-butanal due to the presence of $Mo^{16}O_t \approx 8$ % (Table 5, expt 1). The assumption of a clean loss of ligand MoO_t with butanal allowed a theoretical isotope pattern for product [Cr, Mo, O_6, H]$^-$ to be generated. The agreement between experimental and theoretical isotope patterns supported this assumption (Figure 7a and b). In contrast, theoretical isotope patterns generated assuming clean loss of either $Cr^{16}O_t$ or CrO_bMo oxo ligands were in much poorer agreement with experiment (e.g., Figure 7c).

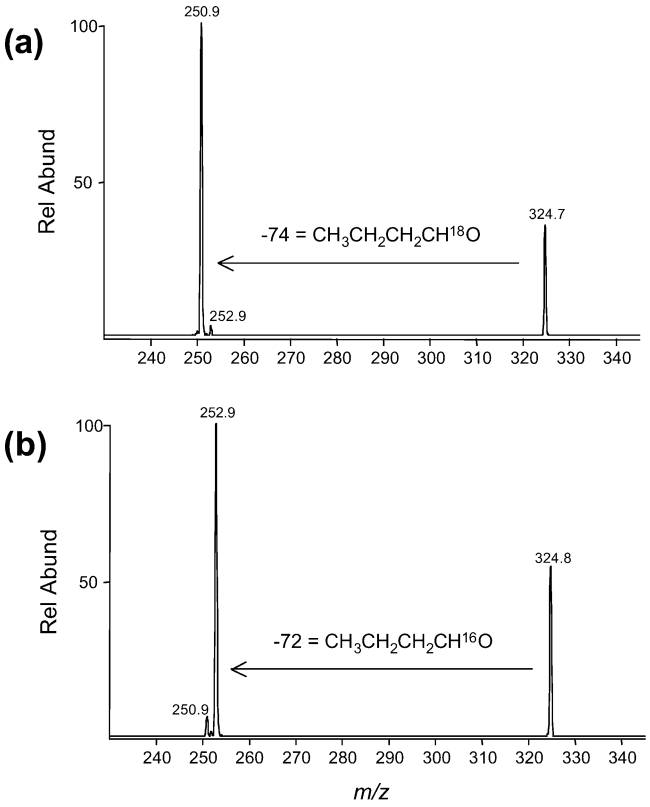

Figure 6. Mass selection and collisional activation of $[CrMoO_6(OBu)]^-$. A single peak (*m*/*z* 325) was isolated in each case. (a) Labeled at MoO_t (92 atom % ^{18}O) (Tables 1 and 5; expt 1). (a) Labelled at CrO_t (92 atom % ^{18}O) (Tables 1 and 5; expt 3).

The observations were consistent with the source of butanal being a terminal butoxo ligand at molybdenum, suggesting alkylation at a molybdenum oxo ligand (Scheme 1). The complementary experiment for $[CrMoO_6(OBu)]^-$ generated from $\{Bu_4N^+[CrMoO_7]^{2-}\}^-$ labeled at chromium (CrO_t, 92; MoO_t, 8 atom % ^{18}O; Table 1, expt 3) resulted in the predominant loss of 72 Da, consistent with loss of ^{16}O-butanal (Figures 6b). The observations were again consistent with the source of butanal being a terminal butoxo ligand at the molybdenum site.

Analogous experiments were carried out for $[CrWO_6(OBu)]^-$ labeled selectively at the terminal oxo ligands of one metal center (Tables 1 and 5; expts 4 and 6; Figures S11 and S12). The observations were entirely equivalent to those described above for $[CrMoO_6(OBu)]^-$ and indicated that the butoxo ligand of $[CrWO_6(OBu)]^-$ is located at a terminal tungsten site.

Reaction of Labeled $[CrMO_6(OBu)]^-$ with Alcohol. $[CrMoO_6(OBu)]^-$ and $[CrWO_6(OBu)]^-$ reacted with alcohols ROH with loss of butanol to form $[CrMoO_6(OR)]^-$ and $[CrWO_6(OR)]^-$, respectively (eq 6). This reaction was also used to investigate the site of the butoxo ligand in selectively labeled $[MM'O_6(OBu)]^-$.

$[CrMoO_6(OBu)]^-$ reacted extremely slowly with methanol ($k \approx 4 \times 10^{-14}$ cm^3 molecule^{-1} s^{-1}; Table 2) but more rapidly with the more acidic alcohol CF_3CH_2OH ($k = 3.3 \times 10^{-11}$ cm^3 molecule^{-1} s^{-1}). This faster rate of reaction meant that lower concentrations of alcohol were required, and allowed for improved instrument resolution. Reaction

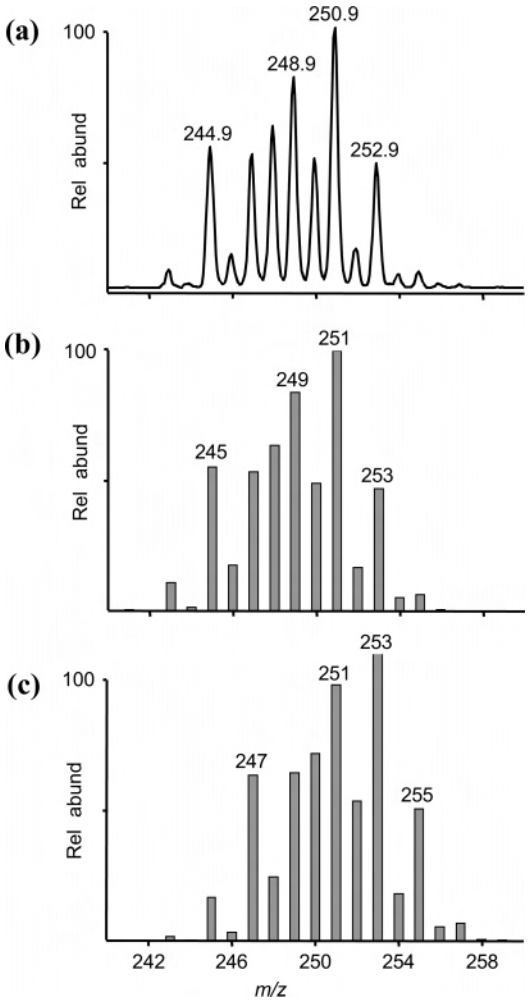

Figure 7. Experimental and theoretical isotope patterns for product $[Cr,Mo,O_6,H]^-$ generated by collisional activation of $[CrMoO_6(OBu)]^-$ labeled at MoO_t (92 atom % ^{18}O; Tables 1 and 5; expt 1): (a) experimental; (b) theoretical pattern assuming clean loss of MoO_t with butanal; (c) theoretical pattern assuming clean loss of CrO_t with butanal.

of CF_3CH_2OH with $[CrMoO_6(OBu)]^-$ labeled at molybdenum (MoO_t, 92 atom % ^{18}O, Tables 1 and 5; expt 1) led to loss of ^{18}O-butanol (Figure 8a). This was consistent with elimination of a labeled molybdenum oxo ligand with butanol. A theoretical isotope pattern for product $[CrMoO_6(OCH_2CF_3)]^-$ based on the assumption of loss of MoO_t with butanol was in good agreement with experiment, consistent with this conclusion (Figure 9a and b). The complementary experiment for the equivalent anion labeled at chromium led to loss of ^{16}O-butanol (Figure 8b, Figure S16). The observations indicated the presence of a terminal butoxo ligand at molybdenum, and are consistent with conclusions from the loss of butanal from these species. Equivalent experiments for selectively labeled $[CrWO_6(OBu)]^-$ indicated the presence of a terminal butoxo ligand at tungsten (Figures S17 and S18), again in agreement with conclusions from loss of butanal.

Proton Mobility in $[CrMoO_6(OH)]^-$. The heteronuclear anions $[MM'O_6(OH)]^-$ exhibited significant differences in rate of reaction toward methanol compared with their homonuclear counterparts (eq 4; Table 2). This suggested an investigation into the site of reaction in these species

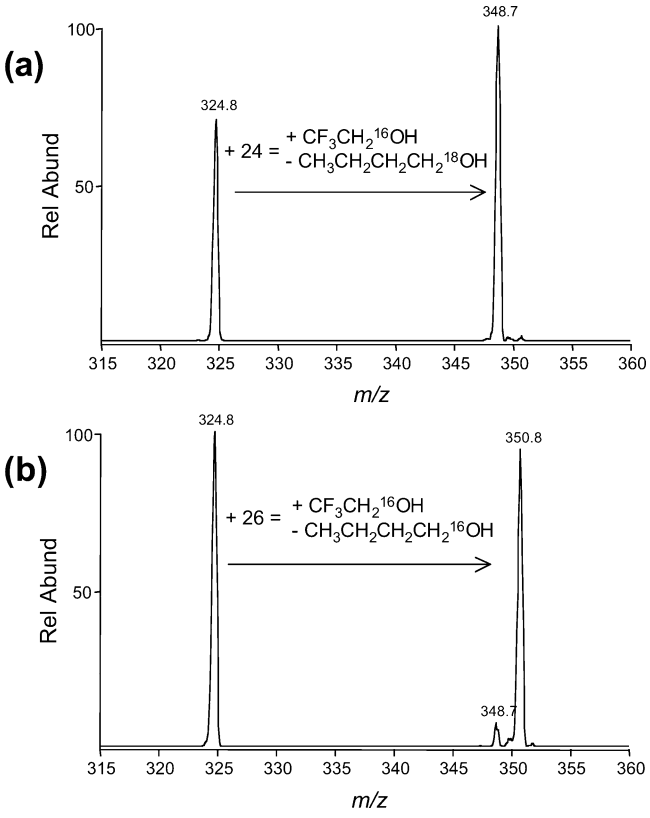

Figure 8. Mass selection and reaction of $[CrMoO_6(OBu)]^-$ with CF_3CH_2OH. A single peak (*m*/*z* 325) was isolated in each case: (a) labeled at MoO_t (92 atom % ^{18}O) (Tables 1 and 5; expt 1), and (b) labeled at CrO_t (92 atom % ^{18}O) (Tables 1 and 5; expt 3).

analogous to that described above for $[CrMoO_6(OBu)]^-$ and $[CrWO_6(OBu)]^-$.

$[CrMoO_6(OH)]^-$ labeled at chromium was generated from solutions of ^{18}O labeled $[CrO_4]^{2-}$ and unlabeled $[MoO_4]^{2-}$ in a manner analogous to that described above for $[CrMoO_6(OBu)]^-$ (Tables 1 and 5; expt 3). Estimates of label incorporation equivalent to those for $[CrMoO_6(OBu)]^-$ provided good agreement between experimental and theoretical isotope patterns for $[CrMoO_6(OH)]^-$ (CrO_t, 92; MoO_t, 8; CrO_bMo, 90 % ^{18}O; Figure S19). The more acidic alcohol CF_3CH_2OH was again used to allow for lower concentrations of alcohol and improved instrument resolution. $[CrMoO_6(OH)]^-$ labeled at chromium reacted with CF_3CH_2OH with loss of water to form a product ion assigned to $[CrMoO_6(OCH_2CF_3)]^-$. Mass selection and reaction of a single peak demonstrated loss of a mixture of $^{16}OH_2$ and $^{18}OH_2$ (Figure 10). Furthermore, theoretical isotope patterns for product $[CrMoO_6(OCH_2CF_3)]^-$ based on the assumption of clean loss of a terminal chromium, terminal molybdenum, or bridging oxo ligand with water were in poor agreement with experiment (Figure S21). This indicated that oxo ligands from both the chromium and molybdenum centers were eliminated as water.

These data contrasted with the observation of clean loss of an oxo ligand from the molybdenum center in equivalent reactions of $[CrMoO_6(OBu)]^-$ with CF_3CH_2OH (e.g., compare Figures 8a and 10), and indicated that label scrambling had occurred in $[CrMoO_6(OH)]^-$. This meant that the technique of selective labeling was not appropriate to

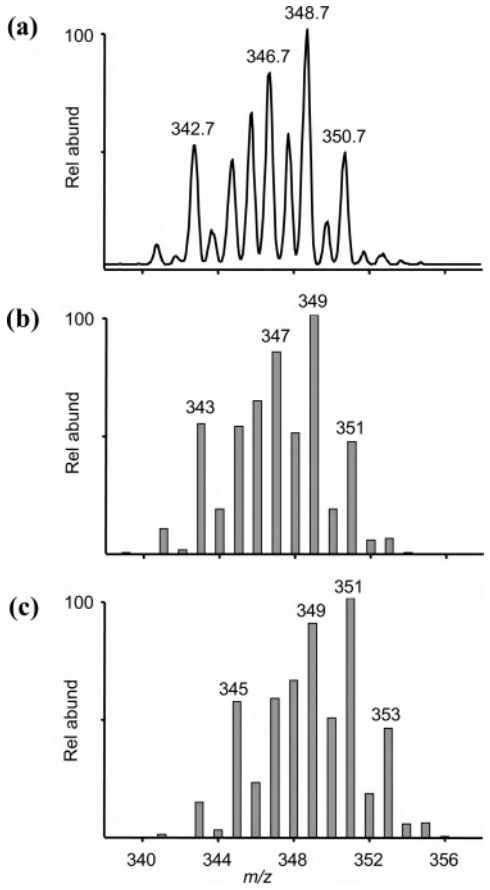

Figure 9. Experimental and theoretical isotope patterns for product $[CrMoO_6(OCH_2CF_3)]^-$ generated by reaction of $[CrMoO_6(OBu)]^-$ labeled at MoO_t (92 atom % ^{18}O; Tables 1 and 5; expt 1) with CF_3CH_2OH: (a) experimental; (b) theoretical pattern assuming the clean loss of MoO_t with butanol; and (c) theoretical pattern assuming the clean loss of CrO_t with butanol.

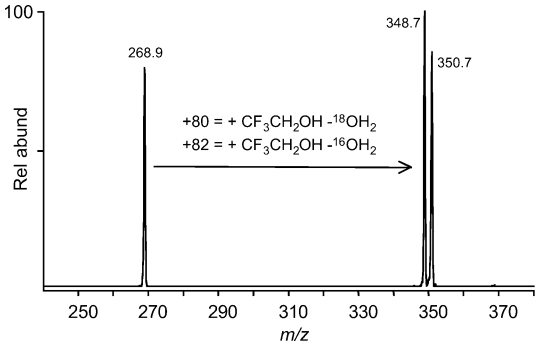

Figure 10. Mass selection and reaction of $[CrMoO_6(OH)]^-$ labelled at CrO_t (92 atom % ^{18}O; Tables 1 and 5; expt 3) with CF_3CH_2OH. The observed mass increases of 80 and 82 Da are consistent with addition of CF_3CH_2OH and loss of a mixture of $^{18}OH_2$ and $^{16}OH_2$, respectively.

investigate the site of reaction in $[MM'O_6(OH)]^-$. This label scrambling might be due to migration of the proton and/or intact hydroxy groups within $[CrMoO_6(OH)]^-$ either prior to or during reaction with alcohol.

Discussion

Formation of $[MM'O_7]^{2-}$. Heterobinuclear anions based upon $[MM'O_7]^{2-}$ were proposed to be formed in a condensation reaction between $[MO_3(OH)]^-$ and $[M'O_3(OH)]^-$ (eq 2). The label incorporation at the bridging oxo ligand in selectively labeled anions might provide insight into the mechanism of formation of these species. For example, estimates for the bridging oxo ligands of $[CrMoO_6(OBu)]^-$ and $[CrWO_6(OBu)]^-$ were close to those estimated for the terminal chromium oxo ligands (Table 5). This might indicate that condensation between $[CrO_3(OH)]^-$ and $[MO_3(OH)]^-$ (M = Mo, W) involves loss of an oxygen of $[MO_3(OH)]^-$ with water (e.g., eq 11; Table 5, expt 1)

$$[CrO_3(OH)]^- + [M^{18}O_3(^{18}OH)]^- \rightarrow [O_3CrOM^{18}O_3]^{2-} + {}^{18}OH_2 \quad (11)$$

Location of Butoxo Ligands. The sites of the butoxo ligands of $[CrMoO_6(OBu)]^-$ and $[CrWoO_6(OBu)]^-$ were established by ^{18}O tracer experiments using both collision-induced dissociation and ion−molecule reactions. Reactions involving ligand loss (Figures 6−9) indicated that the butoxo ligand was terminal and located on the less electronegative center (i.e., Mo or W rather than Cr). These data were also consistent with the theoretical calculations, which indicated a slight preference for Mo or W over Cr (Table 4). In contrast, the H atom and/or OH group of $[CrMoO_6(OH)]^-$ appears to be mobile, precluding isotope labeling experiments using the current methodology (Figure 10).

Information about the site of butoxo ligands in $[CrMO_6(OBu)]^-$ (M = Mo, W) allowed further interpretation of reactivities of related sets of anions. For example, the butoxo ligand is bound to tungsten in both $[CrWO_6(OBu)]^-$ and $[W_2O_6(OBu)]^-$, but the neighboring metal center varies from chromium to tungsten, respectively. This allowed the effect of the neighboring metal center to be evaluated. In contrast, the butoxo ligand is bound to chromium in $[Cr_2O_6(OBu)]^-$ but to tungsten in $[CrWO_6(OBu)]^-$, however the neighboring metal center is chromium in both cases. This allowed the effect of the metal at which the butoxo is bound to be evaluated.

Reaction of $[MM'O_6(OBu)]^-$ with Alcohol. The rates of reaction of $[Cr_2O_6(OBu)]^-$, $[CrMoO_6(OBu)]^-$, and $[Mo_2O_6(OBu)]^-$ with MeOH (eq 6) vary by a factor of at least 2000 in the order $Cr_2 < CrMo \ll Mo_2$ (Table 2). This highlights the important role of both metal centers in this reaction. In particular, the presence of chromium appears to reduce reactivity significantly. For example, the presence of a neighboring chromium in $[CrMoO_6(OBu)]^-$ results in a 500-fold reduction in reactivity relative to that of $[Mo_2O_6(OBu)]^-$ (Table 2). The observed order of reactivity correlates with the basicity of ligand butoxo being diminished by the presence of a neighboring center of greater electronegativity (Cr^{VI}, 3.37 > Mo^{VI}, 2.20).[38] The same trend is observed when Mo is replaced by W (Table 2).

Branching Ratios for Aldehyde/Alkene Elimination. Collisional activation of the butoxo anions $[MM'O_6(OBu)]^-$ led to elimination of butanal or butene (eqs 8 and 9), with the detailed observations dependent on both metal centers (Table 3). Each of the anions containing Cr favored the redox loss of butanal, consistent with the stronger oxidizing power

of Cr^{VI}.[41] In particular, the butoxo ligand of both $[CrWO_6(OBu)]^-$ and $[W_2O_6(OBu)]^-$ is located at tungsten, yet they exhibit markedly different reactivity. While $[W_2O_6(OBu)]^-$ underwent clean loss of butene, the presence of the neighboring chromium in $[CrWO_6(OBu)]^-$ resulted in the exclusive loss of butanal. This is consistent with a mechanism of formal hydride transfer to the neighboring metal atom if it is sufficiently oxidizing (below). The conclusion is supported by theoretical calculations that suggest close contact of the α-H of the alkoxo ligand with the neighboring metal center (Figure 4), as well as similar deductions based upon both theoretical and experimental work on related condensed phase systems.[42−46]

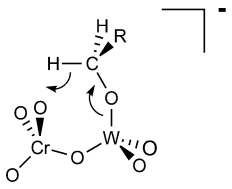

Reaction of $[M, M', O_6, H]^-$ with CH_3NO_2. Neither $[Cr, Mo, O_6, H]^-$ or $[Cr, W, O_6, H]^-$ reacted with nitromethane. This was consistent with the lack of reaction reported previously for $[Cr_2, O_6, H]^-$,[1] and indicated that the presence of chromium in these species prevented reduction of nitromethane. In contrast, $[Mo, W, O_6, H]^-$ exhibited reactive and unreactive components. This was consistent with presence of a reduced hydroxo isomer (reactive component, ∼50%) and an oxidized hydrido isomer (unreactive, ∼50%), equivalent to those proposed previously for the reactive and unreactive components of $[Mo_2, O_6, H]^-$ (∼80 and 20%, respectively).[1] The increased proportion of unreactive component for $[Mo, W, O_6, H]^-$ is consistent with the presence of tungsten favoring the hydride isomer, and also consistent with the presence of only the unreactive hydride isomer for $[W_2, O_6, H]^-$.[1]

Conclusions

Heterobinuclear oxometalate anions based upon $[CrMoO_7]^{2-}$, $[CrWO_7]^{2-}$, and $[MoWO_7]^{2-}$ were generated by the electrospray process from acetonitrile solutions containing two of $(Bu_4N)_2[MO_4]$ (M = Cr, Mo, W) (eq 2). Each of these were tested for the catalytic oxidation of alcohols to aldehydes (Figure 1), and their reactivity compared with that of their homobinuclear counterparts $[M_2O_7]^{2-}$.[1]

Each of the protonated anions $[MM'O_6(OH)]^-$ (M = Mo, W; M ≠ M′) reacted with methanol with loss of water to form $[MM'O_6(OCH_3)]^-$ at a rate that was intermediate between those of $[M_2O_6(OH)]^-$ and $[M'_2O_6(OH)]^-$ (eq 4; Table 2). For example, the presence of chromium in $[CrMoO_6(OH)]^-$ and $[CrWO_6(OH)]^-$ induced a dramatic decrease in reactivity relative to that of $[Mo_2O_6(OH)]^-$ and $[W_2O_6(OH)]^-$, respectively. Collisional activation of the ion-pairs $\{Bu_4N^+[MM'O_7]^{2-}\}^-$ provided access to the butoxo anions $[MM'O_6(OBu)]^-$. Collisional activation of these butoxo anions resulted in either the loss of butanal (redox reaction) or the loss of butene (elimination reaction), with the detailed observations depending on the nature of both M and M′ (eqs 8 and 9; Table 3). For example, $[MoWO_6(OBu)]^-$ eliminated a mixture of butanal (∼80%) and butene (∼20%), consistent with the loss of butanal from $[Mo_2O_6(OBu)]^-$ but butene from $[W_2O_6(OBu)]^-$. The product ions from loss of butanal correspond to ions of stoichiometry $[M, M', O_6, H]^-$, and the reactivity of each of these toward nitromethane was examined (Figure 1). Neither $[Cr, Mo, O_6, H]^-$ nor $[Cr, W, O_6, H]^-$ reduced nitromethane, consistent with a similar lack of reaction observed for $[Cr_2, O_6, H]^-$ and the presence of chromium in each species. In contrast, approximately 50% of the $[Mo, W, O_6, H]^-$ ion population reacted with nitromethane to form $[MoWO_6(OH)]^-$, while the remaining 50% was unreactive. This was consistent with the presence of isomeric forms corresponding to a reduced hydroxo isomer $[MoWO_5(OH)]^-$ (reactive) and an oxidized hydrido isomer $[MoWO_6(H)]^-$ (unreactive), equivalent to those proposed previously for $[Mo_2, O_6, H]^-$.[1]

The site of reaction in the butoxo species $[CrMoO_6(OBu)]^-$ and $[CrWO_6(OBu)]^-$ was investigated by selective labeling of the oxo ligands of one metal center only. The experiments suggested the butoxo ligand was located at Mo and W, respectively. These structural insights allowed a more detailed comparison with the related homobinuclear centers, and highlighted the significant effect of the neighboring metal center in both reaction with methanol and elimination of butanal. For example, the presence of a neighboring Cr in $[CrWO_6(OBu)]^-$ compared with W in $[W_2O_6(OBu)]^-$ resulted in a 100 fold reduction in reactivity toward methanol, and a preference for the elimination of butanal rather than butene.

Acknowledgment. T.W. acknowledges the support of an Australian Postgraduate Award and an award from the Loxton bequest. R.A.J.O. thanks the Australian Research Council for financial support (grant A00103008). Support of the Victorian Institute for Chemical Sciences High Performance Computing Facility is gratefully acknowledged.

Supporting Information Available: Cartesian coordinates for isomers of $[MM'O_6(OCH_3)]$ (Figures S1−S3) and mass spectra illustrating isotope patterns and reactions of selectively labeled species (Figures S4−S21) (pdf). This material is available free of charge via the Internet at http://pubs.acs.org.

IC050288Z

(41) See for example a frost diagram for the chromium group: Shriver, D. F.; Atkins, P. W. *Inorganic Chemistry*, 3rd ed.; Oxford University Press: Oxford, 1999; p 294.
(42) Allison, J. N.; Goddard, W. A., III *J. Catal.* **1985**, *92*, 127−135.
(43) Iwasawa, Y.; Sato, Y.; Kuroda, H. *J. Catal.* **1983**, *82*, 289−298.
(44) Iwasawa, Y.; Yamagishi, M. *J. Catal.* **1983**, *82*, 373−381.
(45) Iwasawa, Y.; Asakura, K.; Ishii, H.; Kuroda, H. *Z. Phys. Chem.* **1985**, *144*, 105−115.
(46) Iwasawa, Y. Inorganic oxide-attached metal catalysts. In *Tailored Metal Catalysts*; Iwasawa, Y., Ed.; D. Reidel Publishing Company: Dordrecht, The Netherlands, 1986; pp 1−85.